Novel Detection of Placental Insufficiency by Magnetic Resonance Imaging in the Nonhuman Primate

Jamie O. Lo, MD[1], Victoria H. J. Roberts, PhD[2], Matthias C. Schabel, PhD[3], Xiaojie Wang, PhD[4], Terry K. Morgan, MD, PhD[5], Zheng Liu, PhD[4], Colin Studholme, PhD[6], Christopher D. Kroenke PhD[3,7], and Antonio E. Frias, MD[1,2]

Abstract

The placenta is a vital organ necessary for healthy fetal development. Placental insufficiency creates an in utero environment where the fetus is at risk of insufficient oxygen or nutrient exchange. This is primarily caused by impairment of either maternal or fetal circulation or vascular thrombosis such as placental infarction. As a result of placental dysfunction, affected fetuses may be growth restricted, neurologically impaired, and at risk of increased morbidity and mortality. In a cohort of 4 pregnant Rhesus macaques, we describe antenatal detection of naturally occurring intrauterine growth restriction (IUGR) and aberrant fetal neurodevelopment in 1 animal. Abnormal growth parameters were detected by Doppler ultrasound, and vascular insufficiency in the intervillous space was characterized by dynamic contrast-enhanced magnetic resonance imaging (DCE-MRI). Furthermore, placental oxygen reserve was shown to be reduced compared to control animals by measurements of placental water T_2^*. To characterize the effects of IUGR on fetal brain development, T_2 and diffusion anisotropy images of the fetal brain were acquired in utero. Reduced brain volume and cerebral cortical surface area were apparent macroscopically. Microstructural abnormalities within the developing white matter and cerebral cortex were also observed through analysis of water diffusion anisotropy. After delivery by cesarean section, pathological examination confirmed placental insufficiency with hypoxia. These findings exemplify how DCE-MRI and T_2^*-based measurements of blood oxygenation within the placenta can provide noninvasive imaging methods for assessing in vivo placental health to potentially identify pregnancies affected by placental insufficiency and abnormal fetal neurodevelopment prior to the onset of fetal and neonatal distress.

Keywords

nonhuman primate, noninvasive imaging, placental insufficiency, intrauterine growth restriction, fetal brain development, MRI

Introduction

Intrauterine growth restriction (IUGR) is one of the leading causes of perinatal mortality and morbidity.[1] Infants born with IUGR are at increased risk of neurological impairment and long-term neurodevelopmental disorders.[2-5] A key contributor to IUGR is placental dysfunction,[6] which is not surprising, since the placenta occupies a central role in facilitating nutrient exchange from mother to fetus.

Doppler ultrasound (Doppler-US) is an established clinical standard for antenatal surveillance, given its safety profile, cost, and ease of accessibility. It has the ability to evaluate abnormal placentation and to semi-quantitatively measure uterine blood flow for the assessment of fetal well-being. However, this approach is constrained to characterizing major maternal blood vessels supporting the placenta and is not capable of assessing blood flow within the intervillous space, the site of nutrient exchange with the fetal vasculature. Limitations in

[1] Department of Obstetrics and Gynecology, Oregon Health & Science University, Portland, OR, USA
[2] Division of Reproductive & Developmental Sciences, Oregon National Primate Research Center, Beaverton, OR, USA
[3] Advanced Imaging Research Center, Oregon Health & Science University, Portland, OR, USA
[4] Division of Neuroscience, Oregon National Primate Research Center, Portland, OR, USA
[5] Department of Pathology, Oregon Health & Science University, Portland, OR, USA
[6] Division of Neonatology, University of Washington, Seattle, WA, USA
[7] Department of Behavioral Neuroscience, Oregon Health & Science University, Portland, OR, USA

Corresponding Author:
Jamie O. Lo, Department of Obstetrics and Gynecology, Oregon Health & Sciences University, 3181 SW Sam Jackson Park Road, Mail Code L466, Portland, OR 97239, USA.
Email: loj@ohsu.edu

existing methods for monitoring placental function in vivo, in combination with a high prevalence of placental insufficiency, highlight the need for a greater understanding and ability to detect placental dysfunction in utero. Magnetic resonance imaging (MRI) is a complementary noninvasive imaging modality that can be used throughout pregnancy.[7,8]

Recently, we have developed MRI-based methods for noninvasively characterizing maternal blood flow and oxygen exchange between the maternal and the fetal vasculature throughout the nonhuman primate (NHP) placenta.[9,10] Blood flow is measured using dynamic contrast-enhanced MRI (DCE-MRI), which requires intravenous administration of an MRI contrast reagent.[9] Oxygen exchange can be quantified through analysis of water T_2^* values via the blood oxygen–level-dependent (BOLD) effect, which is an endogenous mechanism of MRI contrast.[11] Thus, T_2^* measurements offer the potential of future clinical use in humans.

Recent advances in neuroimaging have revealed alterations in normal brain development in the setting of IUGR.[2-5] As the fetal brain develops throughout gestation, it requires substantial nutrient support.[7,12] Although the placenta provides oxygenation and transit of essential metabolites for normal fetal nervous system development, little is known about mechanistic links between placental insufficiency and perturbations to brain development. Retrospective motion correction in MRI has advanced the ability to acquire high-resolution 3-D brain MRI to characterize fetal brain growth in utero.[13] Further, these image reconstruction techniques have been extended to diffusion-based MRI contrast,[14-16] which enables development on the cellular level to be monitored. Studies using both human neonates[17,18] and animal models[19] have identified deficiencies in brain growth and cellular-level maturation, with specific emphasis on the development of the cerebral cortex,[17] associated with IUGR. Incorporation of fetal brain MRI holds promise for gaining new understanding of the role of placental insufficiency in altered brain development observed with IUGR.

Within a control cohort of pregnant Rhesus macaques for a larger study, we detected naturally occurring IUGR secondary to placental insufficiency using Doppler-US as well as MRI modalities, with validation by histological analysis of placental tissue postdelivery. Detailed fetal brain MRI measurements and analyses were also performed to characterize the effect of IUGR on brain development. Together, these measurements provide an assessment of the potential use of newly developed MRI methods for identifying and characterizing placental insufficiency, with specific focus on blood flow and oxygen exchange within the intervillous space. Further, this approach provides the opportunity to determine the consequences of placental insufficiency on brain growth and maturation.

Methods

Experimental Design

A cohort of time-mated pregnant control Rhesus macaques (n = 4) for a larger study were maintained on a diet of standard chow with 14% of calories from fat. All animals completed a prenatal ultrasound at gestational day 50 (G50, the gestational term is 168 in this species) to measure the biparietal diameter. At G135, all animals underwent Doppler-US in addition to fetal brain and placental DCE-MRI and BOLD measurements at gestational day 135 (G135, the gestational term is 168 days in this species) followed by immediate cesarean section delivery. Placental and fetal brain tissues were collected, weighed, and measured postdelivery.

Imaging

Doppler-US. All G50 prenatal ultrasounds were performed on awake animals. Prior to the G135 Doppler-US, animals were sedated by intramuscular administration of 10 mg/kg ketamine. Sedation was maintained on a portable anesthesia delivery system providing O_2 with 1.5% isoflurane. Doppler-US measurements were collected by a sonographer using image-directed pulsed and color Doppler equipment (General Electric Voluson 730, Austria) with a 5- to 9-MHz sector probe. The lowest high-pass filter level was used (100 Hz), and an angle of 15° or less between the Doppler beam was deemed acceptable. Blood flow velocity waveforms were obtained from the proximal portion of the uterine artery (Uta) as described previously.[20-22] Doppler waveform measurements for the Uta and umbilical artery were performed using machine-specific software, and the following measurements were obtained: pulsatility index, velocity–time integral (VTI), and fetal heart rate (HR). The diameter of the Uta was measured using power angiography as previously described.[20-22] The cross-sectional area (CSA) of the vessel was calculated as CSA = π (diameter/2).[2] Uterine artery volume blood flow (cQ$_{Uta}$) was calculated using the following formula and corrected by maternal weight: cQ$_{Uta}$ = VTI × CSA × HR. For the placental volume blood flow (cQ$_{UV}$), the Doppler waveforms were obtained from the straight portion of the intra-abdominal umbilical vein (UV) as described previously.[20-23] The mean velocity (V$_{mean}$) was calculated as 0.5 of the maximum velocity. cQ$_{UV}$ was calculated as: V$_{mean}$ × CSA × 60.

Magnetic resonance imaging. Immediately following the G135 ultrasound procedures, MRI studies were performed on a NHP-dedicated 3-T Siemens TIM-Trio scanner (Siemens, Erlangen, Germany) using a circularly polarized transmit and 15-channel receive radiofrequency "extremity" coil (QED, Cleveland, OH). Following localization of the placenta and acquisition of T_2-weighted half-Fourier acquisition single-shot turbo spin-echo anatomic images in the coronal and axial planes, axial 2-D multislice spoiled gradient echo (SPGR) images (repetition time [TR] = 418 milliseconds, flip angle=30°, 256 × 72 matrix, 96 slices, 1.5 mm isotropic spatial resolution) spanning the entire uterus were acquired at 6 in-phase echo times (echo time [TE] = 4.92, 9.84, 19.68, 29.52, 36.90, and 44.28 milliseconds) with monopolar readout gradients. Subsequently, 3-D SPGR images were acquired in the coronal plane (TR = 9.50 milliseconds, TE = 2.46

milliseconds, $128 \times 56 \times 44$ matrix, 2.5 mm isotropic spatial resolution, flip angles of 3° and 25°), also covering the entire uterus, to allow estimation of T_1 (longitudinal relaxation time) with the variable flip angle (VFA) method.[24] Immediately after acquisition of VFA data, 150 volumes of 3-D SPGR images were acquired for DCE-MRI (TR = 2.00 milliseconds, TE = 0.72 milliseconds, flip angle = 20°, 6/8 partial Fourier encoding in both phase and slab encode directions, elliptical phase undersampling, parallel imaging with generalized autocalibrating partial parallel acquisition [GRAPPA; iPAT factor of 2], acquisition time per frame of 3.64 seconds), with field of view and resolution matched to the VFA images. Ten baseline images were acquired prior to intravenous injection of a standard dose of 0.1 mmol/kg of gadoteridol contrast reagent (Prohance; Bracco Diagnostics Inc, Princeton, New Jersey) at a rate of 30 mL/min using a syringe pump (Harvard Apparatus, Holliston, Massachusetts). Anatomic and multi-echo imaging were performed during expiratory breath holding, achieved by temporarily suspending ventilation, while DCE-MRI data were acquired during ventilated breathing. Relative signal enhancement was computed from the normalized ratio of the signal change with contrast administration to the mean preinjection baseline signal.[25] Physiological monitoring of pulse rate, arterial blood oxygen saturation, and end-tidal CO_2 partial pressure was performed throughout the imaging study, with no deviations from normal ranges observed in these parameters. Each physiological parameter was recorded at 10-minute intervals, and values reported herein are averages over the final 40 minutes of the MRI examination, which overlapped the time period in which placental multi-echo and DCE-MRI data were collected. The BOLD and DCE-MRI analyses were performed as described previously.[9,10] Regions of interest (ROIs) encompassing both the primary and (where present) the secondary lobes of the placenta were drawn on the T_2* maps by visual identification on each image slice.

For anatomical MR examination of the fetal brain, a 2-D turbo spin echo (TSE) sequence was used to acquire T_2-weighted images with the following parameters: TR/TE = 5000/97 milliseconds, GRAPPA factor = 2, and TSE factor = 27. As described previously,[26] multiple contiguous 2-D image stacks, with in-plane resolutions of 0.67 mm and thicknesses of 1 mm, were acquired along the maternal axial, sagittal, and coronal axes to facilitate the reconstruction of a 3-D volume with isotropic resolution. Diffusion-weighted images were acquired using a 2-D spin-echo–based echo-planar imaging (EPI) sequence. One b0 volume and 20 diffusion-weighted volumes (b = 500 s/mm2) were acquired with TR/TE = 5000/93 milliseconds, GRAPPA factor = 2, EPI factor = 78, and echo spacing = 1.09 milliseconds. Similarly, 3 sets of b0 and diffusion-weighted image stacks were acquired along the maternal axial, sagittal, and coronal axes with in-plane resolution of 1.13 mm and thickness of 3 mm. In order to compensate for the relatively poor through-plane resolution for the diffusion data, 3 sets of diffusion-weighted image stacks were acquired along each axis, offset from one another by 1 mm.[26] Reconstruction of T_2-weighted and diffusion MR image stacks were carried out following the procedures summarized by Wang et al,[27] yielding T_2-weighted volume with 0.5 mm isotropic resolution and maps of fractional anisotropy (FA) in water diffusion with 0.75 mm isotropic resolution.

For the analysis of FA within white matter (WM), a template-based ROI approach was used. Template G135 T_2-weighted images were constructed from in utero images acquired from 5 additional control fetuses at G135 following identical procedures to those used for this study (manuscript in preparation). Skull stripping of all images was performed manually using ITK-SNAP (http://www.itksnap.org). An unbiased T_2-weighted brain template was constructed from the 5 skull-stripped T_2-weighted images following procedures of Scott et al,[28] utilizing the ANTS software package (http://stnava.github.io/ANTs/) for all linear and nonlinear image registration and image transformation steps. For 4 of the 5 fetuses, diffusion MRI data were also available, and for these fetuses, the skull-stripped b = 0 image was nonlinearly registered to the T_2-weighted image for that individual. Additionally, each T_2-weighted image was nonlinearly registered to the T_2 template. Thus, an average FA map was generated by transforming each of the 4 individual FA maps to the T_2-weighted template space by applying the parameters from the 2 transforms that link the b = 0 image to the individual T_2-weighted image and the individual T_2-weighted image to the T_2 template. The ROIs were delineated for 8 WM structures on the average FA map (genu, body, and splenium of the corpus callosum, the anterior commissure, anterior and posterior limbs of the internal capsule, the cingulum bundle, and the optic radiations) as illustrated for a subset of ROIs in Figure 1G and H. The FA maps for the IUGR case and 3 G135 control fetuses were nonlinearly registered to the average FA map, and the label map of the 8 WM ROIs was transformed to the individual FA map space using the resulting registration parameters with nearest neighbor interpolation. Reported FA values reflect the mean FA for all image voxels overlapped by the labeled ROI. For all bilateral structures, FA values were averaged between the left and right sides.

For the analyses of the cerebral cortex, surface models of the interface between CSF and cortical gray matter (the pial cortical surface) was generated using the CARET software package (http://brainvis.wustl.edu). Surface area of each hemisphere was measured using a standard CARET function. Cerebral cortical FA mapped onto the cerebral cortical surfaces following previously described procedures.[29,30]

Histologic Analyses

Representative placental samples were collected from each individually identified and mapped cotyledon, fixed in 10% zinc formalin and embedded in paraffin. Histological sections (5 μm) were stained for hematoxylin and eosin and scored by a placental pathologist (T.K.M.) blinded to treatment group for characteristic features of placental insufficiency such as infarctions, knotting, and accelerated villous maturation.
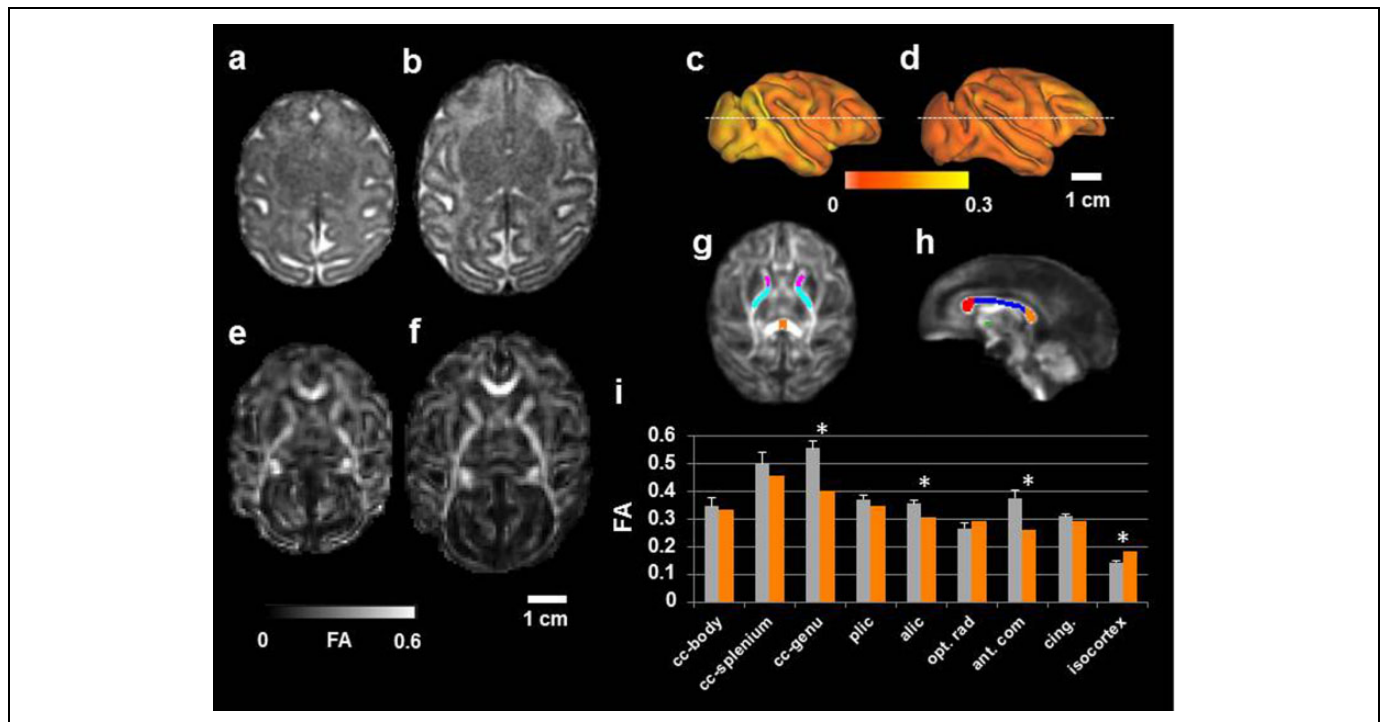
Figure 1. Impaired brain development in the intrauterine growth restriction (IUGR) fetus compared to gestational controls. An axial slice from 3-dimensional (3D) T_2-weighted magnetic resonance imaging (MRI) data reconstructed at (0.5 mm)3 resolution is shown for (A) the IUGR case and (B) a G135 control fetus. Cerebral cortical surface models were constructed for the IUGR brain (C) and the G135 control (D). Water diffusion anisotropy is mapped onto the cerebral cortex surfaces and displayed according to the color bar. Maps of FA, reconstructed at (0.75 mm)3 image resolution, are shown for (E) the IUGR fetus and (F) a representative G135 control. In (G) and (H), white matter (WM) regions of interest (ROIs) are overlaid on a fractional anisotropy (FA) template constructed from 4 control G135 fetuses that were not included in this study (corpus callosum genu, body, and splenium are red, blue, and orange, respectively; anterior commisure is green; anterior limb of the internal capsule is magenta; and posterior limb of the internal capsule is cyan). Average FA within each of the WM ROIs, as well as average FA throughout the isocortex, is shown for average (standard deviation) in the mean for control fetuses (gray bars) and the IUGR fetus (orange bars). Asterisks indicate greater than 3 standard deviation differences between control and IUGR. Abbreviations: cc indicates corpus callosum; plic, posterior limb of the internal capsule; alic, anterior limb of the internal capsule; opt. rad., optic radiations; ant. com., anterior commisure; cing, cingulum bundle.

Results

Growth Parameters

Maternal, fetal, and placental weight at the time of delivery were notably smaller in 1 animal compared to the remaining 3 G135 control animals (Table 1). Hereafter, this animal is referred to as the "IUGR case." The IUGR case was a female fetus, and the control animals comprised of 2 female and 1 male fetus. At G50, the fetal biparietal diameter on ultrasound of the IUGR animal was 1.22 cm, which is consistent with a gestational age of 50 days.[30] For reference, the mean (standard deviation) for the remaining 3 control animals was 1.24 (0.02) cm. Subsequently, an ultrasound performed at G135 revealed a smaller fetal biparietal diameter of 3.9 cm, consistent with G114,[31] in the IUGR case compared to 4.5 (0.06) cm in other control animals (Table 1). Additional fetal biometry measurements were also small for the G135 gestational age compared to controls; the fetal abdominal circumference measured 1.17 cm versus 1.4 (0.04) cm, and the femur length was 2.96 cm versus 3.71 (0.19) cm.

Fetal Cord Blood

Fetal cord blood analysis indicated respiratory acidosis with an arterial pH of 6.99 with a base excess of −23 mmol/L in our IUGR case compared to control cord blood with an average arterial pH of 7.12 and base excess of −2 mmol/L.

Placental Perfusion and Oxygenation

By Doppler-US, we demonstrated a reduction both in cQuv and cQuta in the IUGR case compared to controls (Table 1). There was no difference in umbilical artery and Uta pulsatility indices (Table 1). Maternal perfusion of the placental intervillous space was evaluated using MRI, and multiple irregularities were seen in the IUGR case compared to control animals. For the DCE-MRI experiment, maternal perfusion of the bilobed Rhesus placenta was severely attenuated in the IUGR subject. Figure 2 shows images that reflect perfusion for the IUGR case (Figure 2A and B) and for a representative control case (C and D). Each panel is an image of the difference between pre- and

Table 1. D-US and MRI-Based Measurements of Fetal Biometry and Placental Function and Oxygenation in Gestational Day 135 Controls and Placental Insufficiency Animal.

Parameter	Control (n = 3)	Intrauterine Growth Restriction (n = 1)
Umbilical artery PI	1.15 (0.1)	1.05
Uterine artery PI	0.86 (0.3)	0.57
cQuta, mL/min/kg	34 (22)	31
cQuv	2.1 (0.3)	1.7
Placental blood flow, mL/min	558 (189)	231
BPD, cm	4.5 (0.6)	3.9
Fetal weight, g	333 (11)	193
Maternal weight, g	7483 (894)	6750
Placental weight, g	78 (2)	61
Brain weight, g	20 (0.6)	15
Brain volume, cm^3	31 (0.9)	22.3
Brain surface area, cm^3	11.5 (0.4)	8.7

Abbreviations: PI, pulsatility index; BPD, biparietal diameter; VTI, velocity time integral; CSA, cross section of uterine artery = π (diameter/2)2; Vmean, mean velocity = 0.5 × maximum umbilical vein velocity; cQuta, uterine artery blood flow = VTI × CSA × heart rate adjusted for maternal weight; cQuv, placental volume blood flow = (Vmean × CSA × 60)/abdominal circumference.
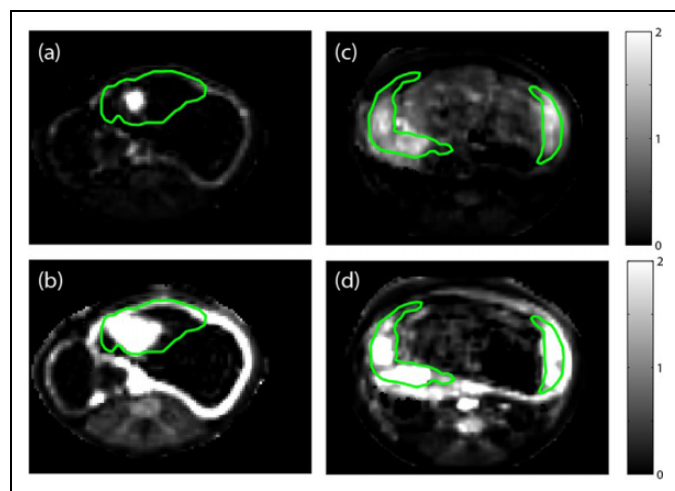

Figure 2. Images showing relative signal enhancement with contrast injection for a single slice through the uterus in a placental insufficiency animal at (A) 30 seconds postinjection and (B) 3 minutes postinjection. Corresponding images in a representative control pregnant Rhesus macaque at (C) 30 seconds postinjection and (D) 3 minutes postinjection. Images are spatially resampled to the T_2* images plotted in Figure 2, with green lines indicating regions of interest (ROIs) drawn by visual identification of the placenta on quantitative T_2* maps.

postcontrast reagent injection, divided by the precontrast reagent injection image. Perfusion of maternal blood through numerous spiral arteries is evident in both lobes of control animals resulting in intensity maxima where contrast reagent concentration is highest. In the IUGR case, perfusion through only 1 spiral artery is apparent in the primary lobe, and the spread of signal intensity enhancement is notably slower. On DCE-MRI, there was minimal quantifiable evidence of spiral artery perfusion of the secondary lobe observed in the IUGR

case (data not shown). Maternal perfusion through spiral arteries is quantified as placental blood flow in Table 1. Consistent with the analysis of cQuta, significantly less maternal blood is supplied to the placenta of the IUGR case because fewer spiral artery sources perfuse the placenta, and the volume flow of blood through these spiral arteries is lower (231 vs 558 mL/min).

In order to assess oxygen supply to the placenta, water T_2* values were analyzed. In G135 control placentas, MR image voxels proximal to spiral artery sources of oxygenated maternal blood are characterized by relatively long T_2* values, as has been previously described for the G110 Rhesus macaque placenta.[10] For MR image voxels further removed from spiral arteries, the concentration of deoxyhemoglobin is higher, due to oxygen exchange with the fetal vasculature, as maternal blood is transported from the spiral artery source throughout the placental intervillous space. The presence of a relatively higher concentration of paramegnetic deoxyhemoglobin causes the water T_2* to be smaller than for voxels near spiral arteries. Comparison of the IUGR case with a representative control animal (Figure 3B and C) shows an overall reduction in T_2* resulting from fewer spiral arteries, which poorly perfuse the organ with oxygenated blood. The histogram (Figure 3A) summarizes T_2* values throughout the 3-D extent of the placenta and indicates an overall distribution of reduced T_2* values in the placental insufficiency case (blue trace) compared to control animals (red traces).

Placental Pathology

Gross placental observations were notable for a large discrepancy in thickness between the 2 placental lobes in the IUGR case: the primary lobe measured 2-cm thick and the secondary lobe measured 0.3-cm thick. Comparatively, the control placentas were notable for a primary lobe measuring 1 (0.01)-cm thick and a secondary lobe measuring 0.8 (0.02)-cm thick. Histologic examination of the IUGR case compared to controls revealed evidence of compensatory growth in the primary lobe with hypermature villi, conspicuous syncytial knots, and areas of infarction (Figure 4B vs A). In addition, the secondary lobe had a paucity of chorionic villi (Figure 4C), and the existing villi were immature for gestational age and lacked fetal capillaries (Figure 4D) confirming aberrant vascular development. These findings are suggestive of relative placental insufficiency in both lobes and an avascular secondary lobe.

Fetal Brain Development

An extensive set of fetal brain measurements were performed on this cohort of pregnant animals, which facilitated a detailed characterization of the state of brain maturation in the IUGR fetus compared to typical G135 fetuses. Retrospective motion correction procedures enabled high-resolution (0.5 mm-sided isotropic voxels) T2-weighted images of the entire fetal brain for the IUGR case (axial view, Figure 1A) and controls (an axial view for a representative brain is shown in Figure 1B).
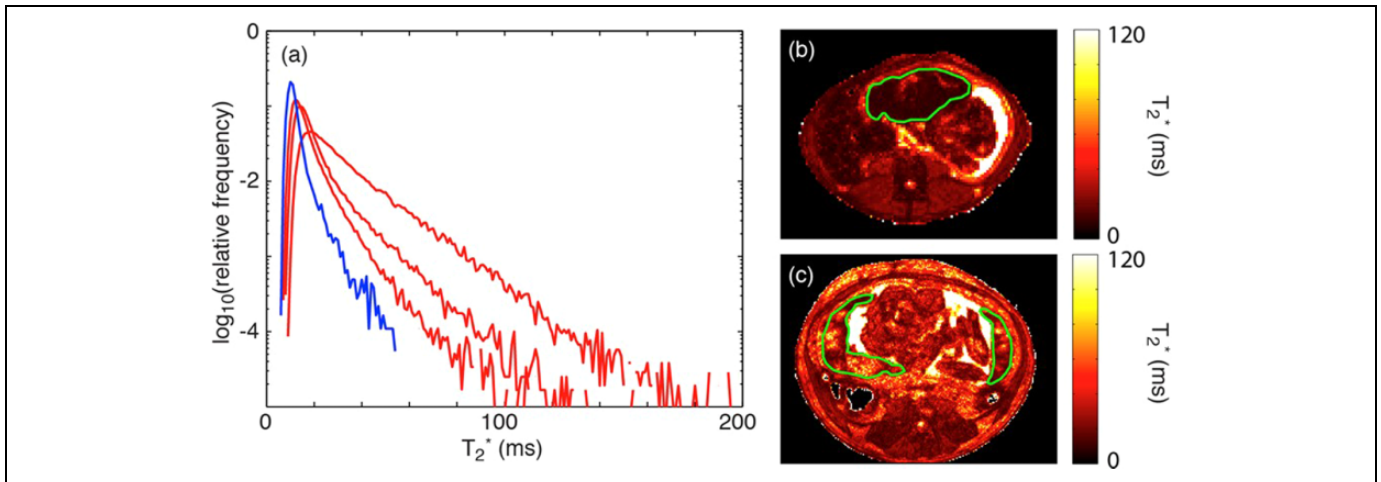
Figure 3. A, Histogram plot of T_2^* versus percentage of placental voxels displayed for our case versus control animals at G135. Our case (blue) had a smaller fraction of large T_2^* values compared to controls (red), demonstrating decreased fetal oxygen availability in the former. B, T_2^* map of placental insufficiency animal. C, T_2^* map of a representative control pregnant Rhesus macaque.
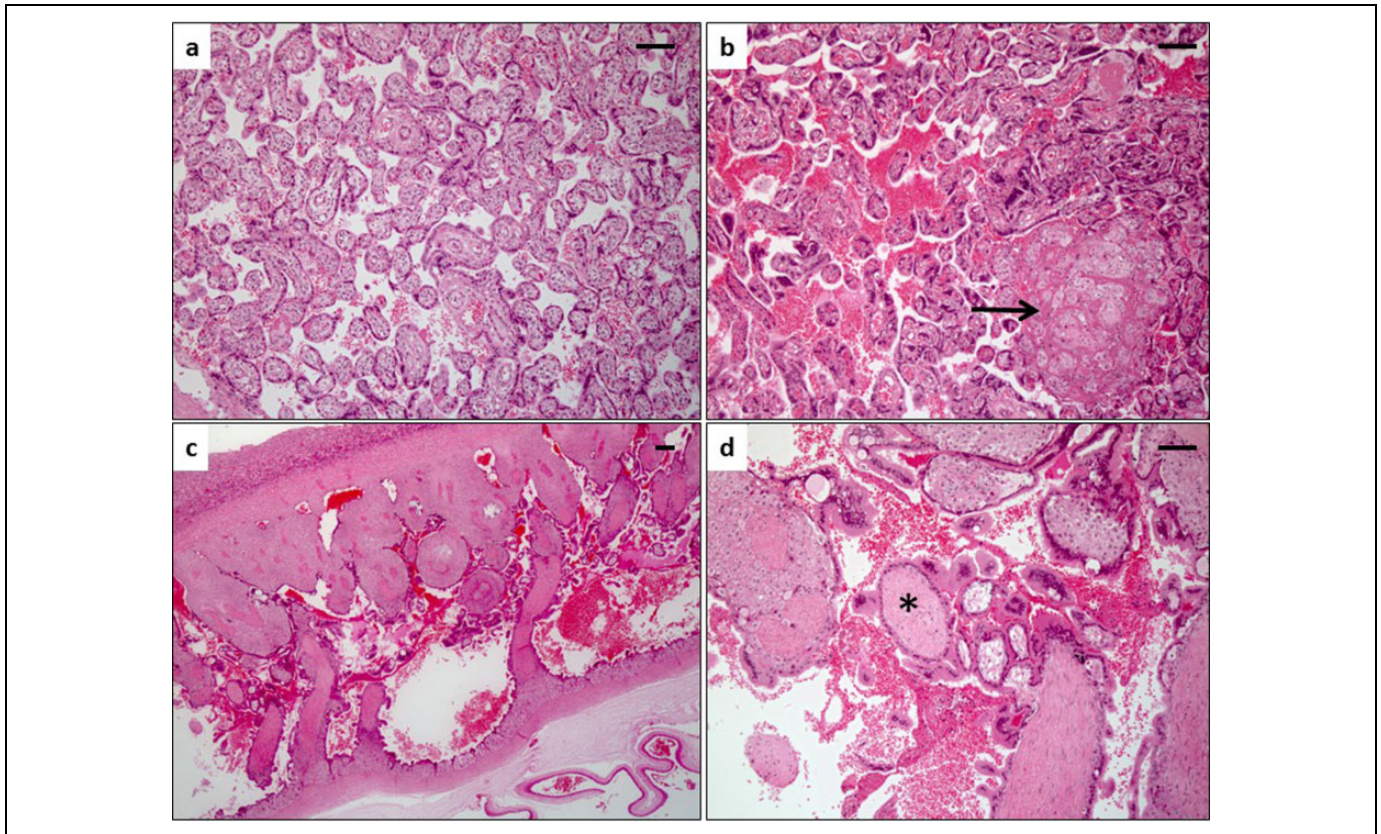

Figure 4. Histopathology of case compared to gestational age G135-matched controls. A, Normal villous histology of a representative Rhesus control placenta at G135 has a predominance of terminal villous differentiation but rare to absent syncytial knots and no gross or microscopic infarctions. B, The primary lobe of the intrauterine growth restriction (IUGR) case showed conspicuous syncytial knotting and infarctions (arrow). C, The secondary lobe of the IUGR animal was very abnormal measuring less than 0.3 cm in thickness with a paucity of chorionic villi. D, Villi in the secondary lobe were also immature for gestational age and lacked fetal capillaries (asterisk). Hematoxylin and eosin–stained histologic sections; bar is 100 mm.

Conspicuous lesions were absent; however, brain volume was smaller (22 mL compared to an average [standard deviation] of 32 [2] mL) in the IUGR case compared to controls, as is evident comparing Figure 1A and B. This was confirmed by measurements of brain weight following delivery (Table 1). The T_2-weighted images were used to generate models of the cerebral

cortical surfaces (Figure 1C, IUGR hemisphere; Figure 1D, representative G135 control hemisphere), and although the overall pattern of cerebral cortical folding was similar to a typical G135 fetal brain, the surface area of the isocortex was reduced (87 cm^2 vs 115 [4] cm^2).

The above-mentioned factors indicate that cerebral growth was perturbed by placental insufficiency. Complimentary information related to the morphological maturation of neurons and glial cells can be inferred from measurements of water diffusion anisotropy. As shown in Figure 1E (IUGR) and F (representative G135 control), it was possible to reconstruct images of FA of water diffusion following retrospective motion correction[26] at 0.75-mm isotropic resolution. Within developing WM, FA increases with age, and reductions in WM FA relative to age-matched controls is typically interpreted as reflecting aberrant development or compromised structural integrity of a WM fiber tract.[32,33] In order to measure FA within multiple major white matter structures, a template-based ROI approach was followed. Within all WM structures characterized by the optic radiation (opt. rad; Figure 1G-I), FA within the IUGR fetus was lower than the mean FA for the corresponding regions in 3 G135 controls. Within the genu of the corpus callosum, anterior commissure, and anterior limb of the internal capsule, FA in the IUGR case was more than 3 standard deviations of the G135 control distribution lower than the mean value observed for controls (Figure 1I, asterisks).

Throughout the cerebral cortical gray matter, water diffusion anisotropy is higher in the placental insufficiency case compared to control animals. This can be appreciated in the lateral views of right hemispheres (Figure 1C and D), in which cerebral cortical FA is projected onto the surface and color coded such that yellow indicated higher values of FA and orange is lower. On average, cortical FA in the IUGR case is 0.182 compared to 0.142 (0.006) for the 3 G135 brains. Higher diffusion anisotropy within cortical gray matter is consistent with less developed dendritic arbors and indicates a lesser degree of morphological differentiation of cells within the cerebral cortex of the growth-restricted fetus compared to the control group.

Discussion

The placenta serves a critical role in the maintenance of a healthy pregnancy and normal fetal growth and development. When normal placental development does not occur, it can result in inadequate fetal nutrition and oxygenation leading to complications such as IUGR with increased fetal and neonatal morbidity and mortality. Our findings highlight the ability of DCE-MRI, as well as the analysis of T_2*, as complementary noninvasive imaging techniques to standard Doppler-US assessment of blood flow in major supporting vessels, with information related to perfusion directly in the intervillous space and exchange of oxygen with the fetal vasculature.

Multiple lines of evidence indicate that the mechanism of action of IUGR characterized in this study is secondary to placental dysfunction, which resulted in abnormal placental blood flow, oxygenation, and nutrient delivery. As the second-trimester G50 ultrasound noted a biparietal diameter appropriate for gestational age in our IUGR case, this suggests that the fetus was not constitutionally small but that this was late-onset pathologic IUGR most commonly secondary to placental dysfunction.[34] We had also observed a reduction in UV blood flow, reflected by a decreased cQuv (Table 1), which is suggestive of diminished oxygen delivery to the fetus. Our findings are also supported by the respiratory acidosis observed in the umbilical cord blood at the time of delivery, which is consistent with what has been previously described in a fetus's metabolic and acid–base response to placental insufficiency.[35] In addition to a decrease in fetal blood supply, alterations in maternal placental hemodynamics were observed on Doppler-US assessment of the Uta Doppler waveforms congruent with prior studies of IUGR.[36] At the interface between the attenuated maternal and fetal perfusion observed in the IUGR case, DCE-MRI measurements confirmed that maternal perfusion of the intervillous space was diminished by approximately a factor of 2 relative to gestational age-matched control animals (Table 1). As a functional consequence of this reduced perfusion, oxygen delivery to the fetus was reduced, as reflected in reduced average placental water T_2* in the IUGR case compared to controls. Together, these corroborative findings implicate fetal hypoxia secondary to aberrant placental function as contributing to or possibly being responsible for the observed IUGR.

Histologic analyses of placental tissue sections also complemented our observations mentioned earlier. Placental histology was notable for infarctions in the primary lobe and absence of fetal vessels and paucity of chorionic villi that are immature in the secondary lobe, which has been previously described in pregnancies complicated by uteroplacental insufficiency[37] and in placentas delivered preterm[38] or exposed to prenatal nicotine or a Western-style diet.[20,39] In addition, placental histology also supplemented imaging findings of placental growth in response to abnormal maternal avascular adaptations to the secondary lobe. The primary lobe of the IUGR case appears to have compensated by altering its growth trajectory and becoming much thicker, with histological analyses demonstrating hypermature villi and findings consistent with placental insufficiency. We have previously reported similar placental adaptations in a NHP model in which the fetal interplacental bridging vessels were surgically ligated midgestation.[40]

Noninvasive imaging procedures were also used to characterize brain volumetric, morphological, and microstructural abnormalities. As is consistent with previous reports,[17] conspicuous lesions were not apparent in T_2-weighted images in the IUGR case compared to controls. Nevertheless, the IUGR brain volume was 72% that of gestation-matched controls, and the cerebral cortex surface area was similarly reduced (76% of the mean value for control fetuses). Diffusion MRI measurements also demonstrated that the development of several WM fiber tracts was attenuated, which corroborates animal[19] and human[41] MRI studies of individuals affected by IUGR.

Notably, water diffusion anisotropy was markedly increased throughout the cerebral cortex of the IUGR case. In the normally developing brain, cerebral cortical water diffusion anisotropy decreases following migration of neurons to the cortical plate, as dendritic and axonal arbors increase in complexity.[42] Fetal hypoxia, which was observed in our study, has previously been shown to attenuate the development of dendritic arbors, and this manifests as increased diffusion anisotropy in the cortex of affected animals.[43] Animal models of other neurodevelopmental disorders including fetal alcohol spectrum disorder[44] and sensory deprivation[45] have also shown that attenuated dendritic and axonal arbor development results in abnormally high-diffusion anisotropy in the cerebral cortex of affected individuals. Although histological analyses have not been performed on the brains shown in Figure 1, recent work has demonstrated that high-diffusion anisotropy within cortex is associated with immature, poorly differentiated dendritic morphology in the fetal Rhesus macaque brain.[46] Thus, in studies of newborn humans, elevated cortical diffusion anisotropy is recognized to be associated with poor neurological outcomes.[47,48] The IUGR case described here provides an example of an association between placental insufficiency and abnormal maturation of cells within the cerebral cortex.

The placenta has significant functional reserve to maintain adequate fetal nutrient delivery during pregnancy. However, when this functional reserve has been depleted, IUGR and its associated risk of poor pregnancy outcome can result. Thus, it is important to determine a noninvasive method to identify pregnancies at risk of hemodynamic alterations before the fetus is affected. The literature is limited on the role of MRI to identify pregnancies at risk of placental insufficiency and to determine disease severity.[49,50] We have described a case of naturally occurring IUGR and abnormal fetal neurodevelopment resulting from placental insufficiency in a cohort of control animals where we employed advanced MRI techniques and correlated these data with tissue histology. These findings exemplify how DCE-MRI and T_2*-based measurements of blood oxygenation are novel imaging strategies that have translational potential as useful obstetric tools for antenatal surveillance and earlier identification of placental and fetal brain health to facilitate clinical intervention and improve pregnancy outcomes prior to the onset of fetal and neonatal morbidity and mortality.

Authors' Note

Christopher D. Kroenke and Antonio E. Frias contributed equally to this work.

Declaration of Conflicting Interests

Funding

References

1. Bernstein I, Gabbe SG. Intrauterine growth restriction. In: Gabbe SG, Niebyl JR, Simpson JL, Annas GJ, eds. *Obstetrics: Normal and Problem Pregnancies*. 3rd ed. New York, NY: Churchill Livingstone; 1996:863-886.

2. Jarvis S, Glinianaia SV, Torrioli MG, et al. Cerebral palsy and intrauterine growth in single births: European collaborative study. *Lancet*. 2003;362(9390):1106-1111.

3. Bergvall N, Iliadou A, Johansson S, Tuvemo T, Cnattingius S. Risks for low intellectual performance related to being born small for gestational age are modified by gestational age. *Pediatrics*. 2006;117(3):e460-e467.

4. Bernstein IM, Horbar JD, Badger GJ, Ohlsson A, Golan A. Morbidity and mortality among very-low-birth-weight neonates with intrauterine growth restriction. The Vermont Oxford Network. *Am J Obstet Gynecol*. 2000;182(1 pt 1):198-206.

5. Levine TA, Grunau RE, McAuliffe FM, Pinnamaneni R, Foran A, Alderdice FA. Early childhood neurodevelopment after intrauterine growth restriction: a systematic review. *Pediatrics*. 2015; 135(1):126-141.

6. American College of Obstetricians and Gynecologists. ACOG Practice bulletin no. 134: fetal growth restriction. *Obstet Gynecol*. 2013;121(5):1122-1133.

7. Andescavage NN, du Plessis A, Limperopoulos C. Advanced MR imaging of the placenta: exploring the in utero placenta-brain connection. *Semin Perinatol*. 2015;39(2):113-123.

8. Ray JG, Vermeulen MJ, Bharatha A, Montanera WJ, Park AL. Association between MRI exposure during pregnancy and fetal and childhood outcomes. *JAMA*. 2016;316(9):952-961.

9. Frias AE, Schabel MC, Roberts V, et al. Using dynamic contrast enhanced MRI to quantitatively characterize maternal vascular organization in the primate placenta. *Magn Reson Med*. 2015; 73(4):1570-1578.

10. Schabel MC, Roberts VHJ, Lo JO, et al. Functional imaging of the non-human primate placenta with endogenous blood oxygen level-dependent contrast. *Magn Reson Med*. 2016;76(5): 1551-1562.

11. Sorensen A, Peters D, Frund E, Lingman G, Christiansen O, Uldbjerg N. Changes in human placental oxygenation during maternal hyperoxia estimated by blood oxygen level-dependent magnetic resonance imaging (BOLD MRI). *Ultrasound Obstet Gynecol*. 2013;42(3):310-314.

12. Volpe JJ. *Neurology of the Newborn. 5*. Philadelphia, PA: Saunders/Elsevier; 2008.

13. Studholme C. Mapping fetal brain development in utero using MRI: the big bang of brain mapping. *Annu Rev Biomed Eng*. 2011;13:345-368.

14. Jiang S, Xue H, Glover A, Rutherford M, Rueckert D, Hajnal JV. MRI of moving subjects using multislice snapshot images with volume reconstruction (SVR): application to fetal, neonatal, and adult brain studies. *IEEE Trans Med Imaging*. 2007;26(7): 967-980.

15. Jiang S, Xue H, Counsell S, et al. In-utero three dimension high resolution fetal brain diffusion tensor imaging. *Med Image Comput Comput Assist Interv*. 2007;10(pt 1):18-26.

16. Rousseau F, Glenn OA, Iordanova B, et al. Registration-based approach for reconstruction of high-resolution in utero fetal MR brain images. *Acad Radiol*. 2006;13(9):1072-1081.

17. Dubois J, Benders M, Borradori-Tolsa C, et al. Primary cortical folding in the human newborn: an early marker of later functional development. *Brain*. 2008;131(pt 8):2028-2041.

18. Lodygensky GA, Seghier ML, Warfield SK, Tolsa CB, Sizonenko S, Lazeyras F. Intrauterine growth restriction affects the preterm infant's hippocampus. *Pediatr Res*. 2008;63(4):438-443.

19. Eixarch E, Batalle D, Illa M, et al. Neonatal neurobehavior and diffusion MRI changes in brain reorganization due to intrauterine growth restriction in a rabbit model. *PLoS One*. 2012;7(2): e31497.

20. Frias A, Morgan T, Evans A, et al. Maternal high-fat diet disturbs uteroplacental hemodynamics and increases the frequency of stillbirth in a nonhuman primate model of excess nutrition. *Endocrinology*. 2011;152(6):2456-2464.

21. Konje JC, Kaufmann P, Bell SC, Taylor DJ. A longitudinal study of quantitative uterine blood flow with the use of color power angiography in appropriate for gestational age pregnancies. *Am J Obstet Gynecol*. 2001;185(3):608-613.

22. Acharya G, Sitras V, Erkinaro T, et al. Experimental validation of uterine artery volume blood flow measurements by Doppler ultrasonography in pregnant sheep. *Ultrasound Obstet Gynecol*. 2007; 29(4):401-406.

23. Acharya G, Wilsgaard T, Berntsen GK, Maltau JM, Kiserud T. Doppler-derived umbilical artery absolute velocities and their relationship to fetoplacental volume blood flow: a longitudinal study. *Ultrasound Obstet Gynecol*. 2005;25(5):444-453.

24. Schabel MC, Morrell GR. Uncertainty in T(1) mapping using the variable flip angle method with two flip angles. *Phys Med Biol*. 2009;54(1):N1-N8.

25. Schabel MC, Parker DL. Uncertainty and bias in contrast concentration measurements using spoiled gradient echo pulse sequences. *Phys Med Biol*. 2008;53(9):2345-2373.

26. Fogtmann M, Seshamani S, Kroenke C, et al. A unified approach to diffusion direction sensitive slice registration and 3D DTI reconstruction from moving fetal brain anatomy. *IEEE Transactions on Medical Imaging*. 2014;33(2):272-289.

27. Wang X, Pettersson D, Studholme C, Kroenke C. Characterization of laminar zones in the mid-gestation primate brain with magnetic resonance imaging and histological methods. *Front Neuroanat*. 2015;9:147.

28. Scott JA, Grason D, Fletcher E, et al. Longitudinal analysis of the developing rhesus monkey brain using magnetic resonance imaging: birth to adulthood. *Brain Struct Funct*. 2016;221(5): 2847-2871.

29. Kroenke CD, Taber EN, Leigland LA, Knutsen AK, Bayly PV. Regional patterns of cerebral cortical differentiation determined by diffusion tensor MRI. *Cereb Cortex*. 2009;19(12): 2916-2929.

30. Kroenke CD, Van Essen DC, Inder TE, Rees S, Bretthorst GL, Neil JJ. Microstructural changes of the baboon cerebral cortex during gestational development reflected in MRI diffusion anisotropy. *J Neurosci*. 2007;27(46):12506-12515.

31. Tarantal AF, Hendrickx AG. Prenatal growth in the cynomolgus and rhesus macaque (*Macaca fascicularis* and *Macaca mulatta*): a comparison by ultrasonography. *Am J Primatol*. 1988;15(4): 309-323.

32. Mori S, Zhang J. Principles of diffusion tensor imaging and its applications for basic neuroscience research. *Neuron*. 2006;51(5): 527-539.

33. Mukherjee P, McKinstry R. Diffusion tensor imaging and tractography of human brain development. *Neuroimaging Clin N Am*. 2006;16(1):19-43.

34. Faraci M, Renda E, Monte S, et al. Fetal growth restriction: current perspectives. *J Prenat Med*. 2011;5(2):31-33.

35. Baschat AA. Fetal responses to placental insufficiency: an update. *BJOG*. 2004;111(10):1031-1041.

36. North RA, Ferrier C, Long D, Townend K, Kincaid-Smith P. Uterine artery Doppler flow velocity waveforms in the second trimester for the prediction of preeclampsia and fetal growth retardation. *Obstet Gynecol*. 1994;83(3):378-386.

37. Salafia C, Charles A, Maas E. Placental and fetal growth restriction. *Clin Obstet Gynecol*. 2006;49(2):236-256.

38. Morgan T. Role of the placenta in preterm birth: a review. *Am J Perinatol*. 2016;33(3):258-266.

39. Lo J, Schabel M, Roberts V, et al. Vitamin C supplementation ameliorates the adverse effects of nicotine on placental hemodynamics and histology in non-human primates. *Am J Obstet Gynecol*. 2015;212(3):370.e1-e8.

40. Roberts VH, Rasanen JP, Novy MJ, et al. Restriction of placental vasculature in a non-human primate: a unique model to study placental plasticity. *Placenta*. 2012;33(1):73-76.

41. Sizonenko SV, Borradori-Tolsa C, Bauthay DM, Lodygensky G, Lazeyras F, Huppi P. Impact of intrauterine growth restrict and glucocorticoids on brain development: insights using advanced magnetic resonance imaging. *Mol Cell Endocrinol*. 2006; 254-255:163-171.

42. Leigland LA, Kroenke CD. A comparative analysis of cellular morphological differentiation within the cerebral cortex using diffusion tensor imaging. *Neuromethods*. 2010;50:329-351.

43. Dean JM, McClendon E, Hansen K, Azimi-Zonooz A, Chen K, Riddle A. Prenatal cerebral ischemia disrupts MRI-defined cortical microstructure through disturbances in neuronal arborization. *Sci Transl Med*. 2013;5(168):168ra7.

44. Leigland LA, Budde MD, Cornea A, Kroenke CD. Diffusion MRI of the developing cerebral cortical gray matter can be used to detect abnormalities in tissue microstructure associated with fetal ethanol exposure. *Neuroimage*. 2013;83:1081-1087.

45. Bock AS, Olavarria JF, Leigland LA, Taber EN, Jespersen SN, Kroenke CD. Diffusion tensor imaging detects early cerebral cortex abnormalities in neuronal architecture induced by bilateral neonatal enucleation: an experimental model in the ferret. *Front Syst Neurosci*. 2010;4:149.

46. Wang X, Studholme C, Grisgy PL, Frias AE, Cuzon Carlson VC, Kroenke CD. Folding, but not surface area expansion is associated with cellular morphological maturation in the fetal cerebral cortex. *J Neurosci*. 2017;37(8):1971-1983.

47. Ball G, Srinivasan L, Aljabar P, et al. Development of cortical microstructure in the preterm human brain. *Proc Natl Acad Sci USA*. 2013;110(23):9541-9546.

48. Vinall J, Grunae RE, Brant R, et al. Slower postnatal growth is associated with delayed cerebral cortical maturation in preterm newborns. *Sci Transl Med*. 2013;5(168):168ra8.

49. Damodaram M, Story L, Eixarch E, et al. Placental MRI in intrauterine fetal growth restriction. *Placenta*. 2010;31(6): 491-498.

50. Damodaram MS, Story L, Eixarch E, et al. Foetal volumetry using magnetic resonance imaging in intrauterine growth restriction. *Early Hum Dev*. 2012;88(suppl 1):S35-S40.